



Interplay of quantum methyl rotation and crystal structure in the lithium acetate dihydrate: neutron diffraction, inelastic neutron scattering and theory

Béatrice Nicolai^a, Alain Cousson^b, François Fillaux^{a,*}

^a LADIR-CNRS and Université Pierre et Marie Curie, 2 rue H. Dunant, 94320 Thiais, France

^b Laboratoire Léon Brillouin (CEA and CNRS), 91 191, Gif sur Yvette cedex, France

Received 27 November 2002; in final form 17 February 2003

Abstract

The crystal structure of the methyl-deuterated lithium acetate dihydrate, ${}^7\text{LiCD}_3\text{COO} \cdot 2\text{H}_2\text{O}$, has been determined at 300, 40 and 14 K with the single crystal neutron diffraction technique. The probability density distributions of deuterium atoms were obtained by Fourier difference in the plane of the D atoms. At 14 K, the crystal symmetry is *P*man. Methyl-groups are totally ordered and the angular probability density has three sharp peaks. A phase transition to the *C*mmm symmetry occurs at (17.5 ± 0.5) K. This structure is analogous to that of the fully hydrogenated derivative at any temperature. However, the Fourier difference at 40 K reveals six maxima of probability for the D atoms, due to centrosymmetric pairs of face-to-face methyl groups, on the top of a continuous ring due to delocalised or disordered atoms. At 300 K, only the continuous and nearly isotropic distribution survives. In order to analyse the tunnelling spectra obtained with the inelastic neutron scattering technique we introduce symmetry-adapted angular coordinates for the strongly coupled pairs of methyl rotors. The dynamics are represented with in-phase and anti-phase rotation of the two partners. The effective moment of inertia is twice that of a single methyl group. The effective potential barrier with the threefold symmetry for in-phase rotation is ≈ 2 meV for the CH_3 pairs and ≈ 4.5 meV for the CD_3 analogues. These effective potentials are tentatively decomposed into two contributions that favour opposite orientations: the on-site potential and the interaction with next nearest neighbours, respectively. Both temperature and mass effects are rationalised with the mean angular amplitude of the rotors. We can thus account for the crystal phase transition upon methyl deuteration. The potential barrier with the sixfold symmetry for anti-phase rotation is ≈ 32 meV. It does not play any role in the ordering/disordering mechanism.

© 2003 Elsevier Science B.V. All rights reserved.

1. Introduction

Light particles moving in a potential with topological degeneracy manifest their quantum nature via tunnelling. Owing to the spatial extension

* Corresponding author. Tel.: +33-14-97-81283; fax: +33-149-78-1118.

E-mail address: fillaux@glvt-cnrs.fr (F. Fillaux).

of the wave function, the otherwise degenerate ground state in the classical regime split into sub-levels. In the condensed matter, the observation of tunnelling sheds light onto fundamental problems of quantum mechanics in complex environments.

For light quantum rotors like methyl groups, strict topological degeneracy arises from the intrinsic periodicity of the angular coordinate and rotational tunnelling is observed in many crystals at a low temperature [1]. The upper limit of the tunnel splitting is the rotational constant $B = \hbar^2/2I_r$, where I_r is the moment of inertia of the rotor. For an isolated and rigid CH_3 group rotating around its axis of inertia supposed to be fixed, B ranges from 650 to 700 μeV and from 325 to 350 μeV for CD_3 . The magnitude of the tunnel splitting depends on the particle mass and potential shape (distances between identical sites, barrier height,...). Deuteration is of dramatic consequences to tunnelling frequencies.

In many molecular crystals, the frequency range for tunnelling is well separate from the density-of-states of optical phonons and dynamical interaction with the lattice is very weak. Therefore, tunnelling transitions are specific to rotational coordinates and can be represented with rather simple Hamiltonians. For methyl groups, this specificity can be fully exploited with the inelastic neutron scattering (INS) techniques because the cross-section of H atoms for incoherent neutron scattering is much greater than for any other atoms, by about one order of magnitude [2]. Intensity arising from the crystal density-of-states (primarily acoustic phonons in the tunnelling energy range) can be ignored. However, the observation of tunnelling transitions for deuterated analogues is hampered by the much weaker cross-section of D atoms and by the dramatic decrease of the splitting upon deuteration. This information is often lacking and this is a limitation for modelling rotational dynamics.

Pioneering INS works with rather modest resolution [3,4] have first revealed single tunnelling transitions and dynamical coupling between rotors was ignored [5]. With better spectrometer resolution, multi-component spectra due to dynamical coupling were observed and different models were proposed to account for local or

collective rotational dynamics. The diversity of interpretations is partly due to a lack of information and this is a long lasting source of controversy. Unfortunately, the hope that advanced quantum chemistry methods could provide realistic modelling of the effective potentials experienced by methyl rotors is not yet realized [6,7]. Experiments remain the best source of knowledge of these quantum dynamics.

The present paper reports new investigations of a prototypical system for complex dynamics of methyl rotors experiencing rather weak potential barriers: the lithium acetate dihydrate, $\text{LiCH}_3\text{-COO}\cdot 2\text{H}_2\text{O}$ or Liac-h₇. The simultaneous use of complementary techniques (INS and single-crystal neutron diffraction) to measure isotope derivatives provides insight on the relationship between crystal structure and rotational dynamics.

For the fully hydrogenated crystal the symmetry is $Cmmm$ at any temperature between 300 and 1 K [7,8]. The methyl groups are arranged in face-to-face coaxial pairs with their axes parallel to the (*a*) crystal axis (see Fig. 1). The distance between consecutive axes of rotation is $a/2 \approx 3.4 \text{ \AA}$ and the distance between the methyl carbon-atoms within pairs is $0.3b \approx 3.3 \text{ \AA}$. The Fourier difference calculated from single-crystal neutron-diffraction data reveals full delocalisation of the protons in the rotational plane of the methyl groups, even at a very low temperature [7]. In contrast to this, neutron diffraction studies of a powdered sample of the totally deuterated analogue, $\text{LiCD}_3\text{COO}\cdot 2\text{D}_2\text{O}$ or Liac-d₇, have revealed a phase transition from $Cmmm$ to $Pman$ symmetry, with full ordering of the CD_3 groups, that does not occur for the hydrogenated crystal [9]. To the best of our knowledge, there is no model to account for this phase transition induced by deuteration.

From the viewpoint of rotational dynamics, early measurements of the proton spin–lattice relaxation have revealed almost free rotation of the methyl groups [10] and tunnelling transitions were observed with INS below 300 μeV at liquid-helium temperature. The rather complex spectrum for Liac-h₇ was first attributed to coupling between face-to-face coaxial rotors, in accordance with the crystal structure [11–13]. Tunnelling transitions for the methyl-deuterated analogue, LiCD_3COO ,

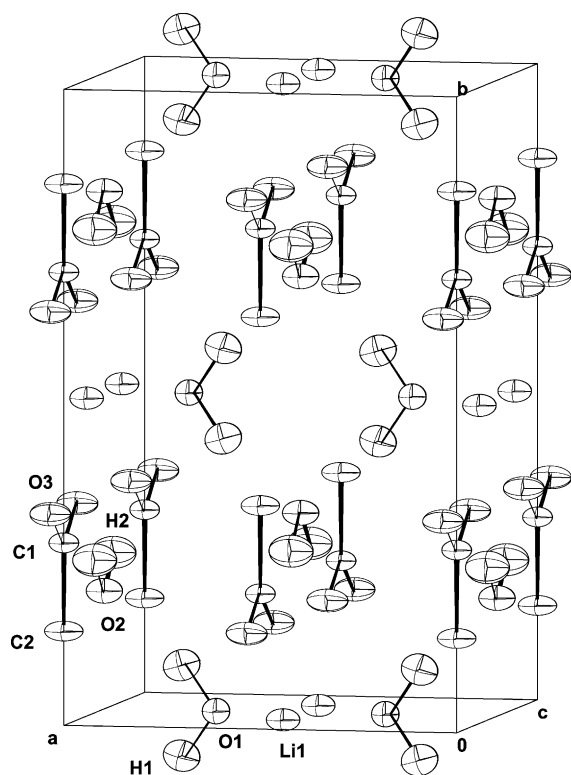


Fig. 1. Schematic view of the crystal structure of $\text{LiCOOCD}_3 \cdot 2\text{H}_2\text{O}$ in the $Cmmm$ phase at 300 K. The disordered deuteron atoms are not represented. Thermal ellipsoids represent 50% probability for atomic positions.

$2\text{H}_2\text{O}$ or $\text{Li}ac\text{-}h_4d_3$, anticipated in the 50 μeV region, were actually observed at $\approx 12.5 \mu\text{eV}$. This decrease of the splitting along with frequency shifts in isotope mixtures containing CH_3 and CD_3 analogues were attributed to a substantial increase of the effective potential barrier upon deuteration [14]. Alternatively, INS spectra of isotope mixtures containing hydrogenated and partially deuterated (CH_2D) analogues were tentatively interpreted in terms of collective rotational dynamics [15], analogous to those reported for the 4-methylpyridine crystal [16]. More recently, quantum chemistry calculations have suggested that dynamical coupling between methyl groups is marginal, whereas strong interaction of methyl rotation with the surrounding water molecules was emphasized [7]. Rotational–translational coupling was proposed to account for the square-like shape of the density

distribution of methyl protons in the rotational plane.

At the present stage, it is unknown whether the phase transition is induced by deuteration of methyl groups or water molecules or both. In order to obtain more information, we have determined with the single-crystal neutron-diffraction technique the structures of the methyl-deuterated salt crystallised with light water (${}^7\text{Li}ac\text{-}d_3h_4$), at 300, 40 and 14 K (see Section 3). The crystal was fully enriched with the ${}^7\text{Li}$ isotope in order to minimise neutron absorption [2]. The phase transition is characterised and the prominent role of methyl deuteration is established. In Section 4, the angular density distributions of the methyl groups obtained from the neutron-diffraction data by Fourier difference are presented. They provide graphic information on the degree of localisation of the rotors. However, they comprise the squared wave function for methyl rotation (related to the shape of the potential function) convoluted with the probability density arising from internal vibrations, lattice modes and, possibly, disorder. These different contributions cannot be unravelled without dynamical models. Conversely, irrelevant models can be safely eliminated if they do not agree with the observed probability densities. The tunnelling spectra analysed in Section 5 gives direct information on rotational levels and wave functions. As none of the dynamical models proposed so far is in accordance with the observations, we propose a new representation of the coupled pair dynamics with symmetry adapted angular coordinates. This yields a comprehensive view of the tunnelling spectra and a mechanism is proposed in Section 6 for the phase transition induced by methyl deuteration.

2. Experimental

The crystal was obtained by slow evaporation of a saturated aqueous solution. A white transparent lozenge-shaped crystal, about 8 mm along the (001) axis and $6 \times 3 \text{ mm}^2$ perpendicular to this direction, was glued on a goniometer head and then oriented and loaded in a standard cryostat.

Neutron-diffraction measurements were performed on the four-circle neutron diffractometer 5C2 ($\lambda = 0.8308 \text{ \AA}$) at the Orphée reactor (Laboratoire Léon Brillouin, Saclay, France,¹ see Table 1 for experimental details).

The structure was analysed with the program CRYSTALS [17] and scattering factors from [18]. We did not observe any extinction due to anisotropy. The absorption coefficient of $\approx 1 \text{ mm}^{-1}$ is very small and related corrections were ignored. All parameters were refined independently (Tables 1–6). In the disordered phase, the distribution of deuterium atoms was represented with a superposition of a continuous ring and localised atoms [17] (see Tables 5 and 6). At 40 K, the ring and the positions of the localized deuterium atoms were refined independently. Statistically, $\approx 50\%$ of the deuterons are distributed almost isotropically. This distribution is analogous to that measured at 300 K. For the other $\approx 50\%$ of deuterons, the localized distribution has marked sixfold symmetry. The R factor is significantly improved with this model (4.14% instead of 10.30%) but the number of parameters is significantly greater.

The INS experiments were carried out at 1.5 K on the time-of-flight spectrometer IN5 at the Institut Laue Langevin (Grenoble, France).² Powders were loaded in a standard cryostat at liquid helium temperature. The frequencies gathered in Table 8 are 20–40 μeV lower than those previously reported. Indeed, we are quite confident about the accuracy of our measurements with the IN5 spectrometer.

Calculations of energy levels and wave functions for periodic potential functions were carried out with a home made double precision computer code. We used a basis set of $N = 40$ symmetric and $N = 40$ antisymmetric wave functions for free rotors, in order to obtain good accuracy for the 10 lower eigenstates. The $N \times N$ matrix elements were calculated according to the recurrence scheme given in [19].

3. Crystal structures

The phase transition from $Cmmm$ (Fig. 1) to $Pman$ (Fig. 2) occurs at $(17.5 \pm 0.5) \text{ K}$ and there is no evidence of hysteresis. In the $Cmmm$ phase, the C–C bonds along the b direction are at the intersection of two mirror planes and the local periodicity of the distribution of D atoms is at least sixfold. One of the mirror planes no longer exists in the $Pman$ phase at low temperature and the C–C bonds are very slightly tilted perpendicular to the (ab) plane. Consequently, the oxygen atoms O4 and O3 of the acetate skeleton become crystallographically inequivalent and the local symmetry of the methyl groups is compatible with threefold periodicity. Apart from their different symmetries, the crystal structures at 14, 40 and 300 K are very similar from the viewpoint of the unit cell parameters and interatomic distances (see Tables 1–4). Therefore, we do not anticipate any significant change of the Born–Oppenheimer potential for methyl rotation.

The structures are virtually identical for Liac-d₇ [9] and ⁷Liac-d₃h₄, although the OD...O bonds between water molecules are slightly longer than the hydrogen bonds. It can be concluded that the ordering of the deuterated methyl groups at low temperature is essentially a mass effect related to the quantum nature of the rotational dynamics.

4. The density distribution of deuterium atoms

The maps calculated in the D₃ rotational plane with the Fourier difference method are graphic views of the nuclear density distribution for the deuterium atoms at different temperatures $P(\theta, T)$ (see Fig. 3). They comprise dynamical and statistical contributions averaged over space and time. The dynamical contribution is not exclusively due to methyl rotation. It is convoluted with the projection onto the rotational plane of the probability densities for all degrees of freedom involving displacements of the methyl groups. In addition to these dynamical distributions, statistical contributions may arise from crystal disorder. Consequently, it is necessary to introduce dynamical models to unravel these contributions.

¹ www-llb.cea.fr.

² www.ill.fr/YellowBook/IN5/welcome.html.

Table 1
Experimental details

	298 K	40 K	14 K
<i>Crystal data</i>			
Cell setting, space group	Orthorhombic, <i>Cmmm</i>	Orthorhombic, <i>Cmmm</i>	Orthorhombic, <i>Pman</i>
<i>a</i> (Å)	6.82 (1)	6.69 (1)	6.69 (1)
<i>b</i> (Å)	10.86 (3)	10.86 (1)	10.87 (1)
<i>c</i> (Å)	6.59 (2)	6.57 (1)	6.56 (1)
<i>V</i> (Å ³)	488.3	477.5	477.4
<i>Z</i>	4	4	4
<i>D_x</i> (mg m ⁻³)	1.43	1.46	1.46
No. of reflections for cell parameters	9	3	4
θ range (°)	14.1 → 15.7	17.8 → 22.3	14.6 → 22.3
<i>Data collection</i>			
No. of measured reflections	1091	1020	1634
No. of independent reflections	654	639	1154
No. of observed reflections	481	562	903
Criterion for observed reflections	<i>I</i> > 3.00σ(<i>I</i>)	<i>I</i> > 3.00σ(<i>I</i>)	<i>I</i> > 3.00σ(<i>I</i>)
<i>R_{int}</i>	0.01	0.03	0.01
θ max (°)	42.5	42.5	42.5
Range of <i>h, k, l</i>	0 → 11; 0 → 18; -11 → 11	0 → 7; 0 → 11; -7 → 7	0 → 10; 0 → 17; -6 → 1
No. and frequency of standard reflections	2 every 450 min	2 every 450 min	2 every 450 min
<i>Refinement</i>			
Refinement on	F	F	F
<i>R</i>	0.0622	0.0414	0.0585
WR	0.0742	0.0441	0.0688
<i>S</i>	0.9453	1.10901	1.0761
No. of reflections	481	562	903
No. of parameters used in refinement	50	68	84
Weighting scheme (Chebyshev polynomial [32])	With 5 parameters: 3.31, -2.93, 2.62, -0.983, 0.107	With 5 parameters: 1.88, -2.00, 0.884, -0.399, -0.548	With 3 parameters: 2.05, 0.384, 1.53
(<i>Δ</i> / <i>σ</i>) _{max}	0.184882	0.001733	0.062636
Δρ _{max}	1.27	2.40	1.27
Δρ _{min}	-1.82	-3.16	-1.82
Extinction method [33] (extinction coefficient)	7 (1)	9.2 (6)	5.1 (4)

The simplest model for methyl rotation is the isolated and rigid rotor in a threefold potential. The Hamiltonian

$$H_1 = -B \frac{\partial^2}{\partial \theta^2} + \frac{V_{03}}{2} (1 - \cos 3\theta) \quad (1)$$

can be transformed into the Mathieu equation [20]. Eigenstates $E_{n\sigma}$ and wave functions $\Psi_{n\sigma}(\theta)$ depend on two quantum numbers: the principal

torsional number n for the harmonic oscillator limit with full degeneracy and a sublevel index σ , which gives the symmetry of the wave function. Owing to the lack of analytical representation, numerical calculations with the variational method were carried out with the basis set of the free rotor [19]. Once eigenstates and wave functions are known, the angular density distribution arising from rotational dynamics is obtained as a function of the sample temperature as

Table 2
Atomic positions, thermal parameters and occupancies at 300 K

Atom	x/a	y/b	z/c	$U_{\text{iso}} (\text{\AA}^2)$	Occupancy	
Li1	0.000	0.500	0.282(1)	0.024	1.00	
C1	0.000	0.287(1)	0.000	0.019	1.00	
C2	0.000	0.148(2)	0.000	0.029	1.00	
O1	0.215(1)	0.500	0.500	0.024	1.00	
O2	0.000	0.186(1)	0.500	0.028	1.00	
O3	0.000	0.341(1)	0.168(1)	0.030	1.00	
H1	0.303(1)	0.571(1)	0.500	0.038	1.00	
H2	0.000	0.240(1)	0.618(1)	0.041	1.00	
	$U_{11} (\text{\AA}^2)$	$U_{22} (\text{\AA}^2)$	$U_{33} (\text{\AA}^2)$	$U_{23} (\text{\AA}^2)$	$U_{13} (\text{\AA}^2)$	$U_{12} (\text{\AA}^2)$
Li1	0.035(3)	0.015(2)	0.022(2)	0.000	0.000	0.000
C1	0.028(1)	0.012(1)	0.019(1)	0.000	0.000	0.000
C2	0.047(1)	0.012(1)	0.028(1)	0.000	0.000	0.000
O1	0.023(1)	0.020(1)	0.028(1)	0.000	0.000	0.000
O2	0.041(2)	0.019(1)	0.023(1)	0.0000	0.000	0.000
O3	0.053(2)	0.016(1)	0.022(1)	−0.004(1)	0.000	0.000
H1	0.041(2)	0.030(2)	0.043(2)	0.000	0.000	−0.003 (1)
H2	0.061(2)	0.032(2)	0.031(2)	−0.004(1)	0.000	0.000

The space group is $Cmmm$ ($Z = 4$) with $a = 6.814(19) \text{\AA}$, $b = 10.864(34) \text{\AA}$ and $c = 6.597(23) \text{\AA}$. (The quantities in parentheses are the estimated standard deviations.)

Table 3
Atomic positions, thermal parameters and occupancies at 40 K

Atom	x/a	y/b	z/c	$U_{\text{iso}} (\text{\AA}^2)$	Occupancy	
Li1	0.000	0.500	0.285(1)	0.008	1.00	
C1	0.000	0.286(1)	0.000	0.004	1.00	
C2	0.000	0.147(1)	0.000	0.008	1.00	
O1	0.217(1)	0.500	0.500	0.006	1.00	
O2	0.000	0.186(1)	0.500	0.007	1.00	
O3	0.000	0.340(1)	0.169(1)	0.007	1.00	
H1	0.307(3)	0.572(1)	0.500	0.019	1.00	
H2	0.000	0.241(2)	0.381(1)	0.020	1.00	
	$U_{11} (\text{\AA}^2)$	$U_{22} (\text{\AA}^2)$	$U_{33} (\text{\AA}^2)$	$U_{23} (\text{\AA}^2)$	$U_{13} (\text{\AA}^2)$	$U_{12} (\text{\AA}^2)$
Li1	0.009(2)	0.005(1)	0.008(2)	0.000	0.000	0.000
C1	0.006(1)	0.002(1)	0.005(1)	0.000	0.000	0.000
C2	0.013(1)	0.002(1)	0.008(1)	0.000	0.000	0.000
O1	0.006(1)	0.005(1)	0.008(1)	0.000	0.000	0.000
O2	0.009(1)	0.004(1)	0.007(1)	0.000	0.000	0.000
O3	0.012(1)	0.003(1)	0.005(1)	−0.001(1)	0.000	0.000
H1	0.020(2)	0.016(2)	0.025(1)	0.000	0.000	−0.005(1)
H2	0.030(2)	0.016(1)	0.015(2)	0.005(2)	0.000	0.000

The space group is $Cmmm$ ($Z = 4$) with $a = 6.692(13) \text{\AA}$, $b = 10.865(15) \text{\AA}$ and $c = 6.568(10) \text{\AA}$. (The quantities in parentheses are the estimated standard deviations.)

$$P_d(\theta, T) = \frac{\sum_{n\sigma} \Psi_{n\sigma}^2(\theta) \exp\left(\frac{-E_{n\sigma}}{kT}\right)}{\sum_{n\sigma} \exp\left(\frac{-E_{n\sigma}}{kT}\right)}. \quad (2)$$

The radial distribution is mainly due to the mean square amplitude of displacements parallel

to the plane of rotation for the D atoms. It is gaussian in shape and can be represented as

$$\rho_r(r, T) = \left(\frac{1}{\pi \langle u_{\text{iso}}^2 \rangle_T}\right)^{1/2} \exp\left[-\frac{(r - r_0)^2}{\langle u_{\text{iso}}^2 \rangle_T}\right]. \quad (3)$$

Table 4
Atomic positions, thermal parameters and occupancies at 14 K

Atom	x/a	y/b	z/c	$U_{\text{iso}} (\text{\AA}^2)$	Occupancy		
Li1	0.000	0.499(1)	0.284(1)	0.006	1.00		
C1	0.000	0.286(1)	0.000(1)	0.003	1.00		
C2	0.000	0.145(1)	-0.005(1)	0.005	1.00		
O1	0.217(1)	0.5000	0.500	0.005	1.00		
O2	0.000	0.186(1)	0.502(1)	0.005	1.00		
O3	0.000	0.339(1)	0.171(1)	0.005	1.00		
O4	0.000	0.341(1)	-0.169(1)	0.005	1.00		
H1	0.306(1)	0.428(2)	0.500(1)	0.019	1.00		
H2	0.000	0.240(1)	0.381(2)	0.019	1.00		
H3	0.000	0.241(2)	0.621(1)	0.019	1.00		
D1	-0.129(1)	0.115(1)	-0.089(1)	0.032	1.00		
D2	0.000	0.107(1)	0.143(1)	0.046	1.00		
	$U_{11} (\text{\AA}^2)$	$U_{22} (\text{\AA}^2)$	$U_{33} (\text{\AA}^2)$	$U_{23} (\text{\AA}^2)$	$U_{13} (\text{\AA}^2)$	$U_{12} (\text{\AA}^2)$	
Li1	0.009(2)	0.004(2)	0.004(2)	0.000(2)	0.000	0.000	
C1	0.004(1)	0.000(1)	0.004(1)	0.000(1)	0.000	0.000	
C2	0.010(1)	0.001(1)	0.006(1)	0.000(1)	0.000	0.000	
O1	0.004(1)	0.003(1)	0.007(1)	0.000(1)	0.000	0.000	
O2	0.007(1)	0.002(1)	0.005(1)	0.000(1)	0.000	0.000	
O3	0.010(1)	0.002(2)	0.004(1)	-0.000(1)	0.000	0.000	
O4	0.008(1)	0.002(1)	0.004(1)	0.000(2)	0.000	0.000	
H1	0.018(2)	0.013(2)	0.025(2)	0.000(1)	0.000(2)	0.005(1)	
H2	0.028(2)	0.015(2)	0.014(2)	0.005(2)	0.000	0.000	
H3	0.027(2)	0.016(2)	0.015(2)	-0.006(2)	0.000	0.000	
D1	0.025(2)	0.015(1)	0.057(2)	-0.003(1)	-0.018(1)	-0.004(1)	
D2	0.113(3)	0.013(2)	0.013(2)	0.005(1)	0.000	0.000	

The space group is $Pman$ ($Z = 4$) with $a = 6.695(2) \text{ \AA}$, $b = 10.867(3) \text{ \AA}$ and $c = 6.563(1) \text{ \AA}$. (The quantities in parentheses are the estimated standard deviations.)

Table 5
The continuous density distributions observed at 300 and 40 K are represented with circular rings

T (K)	x/a	y/b	z/c	R (\AA)	$U_{\text{iso}} (\text{\AA}^2)$	Occupancy
300	0.0000	0.113(1)	0.0000	0.994(4)	0.030(1)	3.00
40	0.000	0.112(1)	0.000	0.954(6)	0.011(1)	1.49(2)

The position ($x/a, y/b, z/c$) of the ring centre, the radius R and the isotropic thermal factor U_{iso} were refined independently.

The variance can be further written as $\langle u_{\text{iso}}^2 \rangle_T = \langle u_{\text{M}}^2 \rangle_T + \langle u_{\text{L}}^2 \rangle_T$. The first term arises from internal vibrations of the methyl groups whereas $\langle u_{\text{L}}^2 \rangle_T$ is the isotropic component of the lattice thermal factors. For the deuterium atoms at 14 K $\langle u_{\text{iso}}^2 \rangle_T = (0.04 \pm 0.01) \text{ \AA}^2$ (see Table 4).

The angular distribution due to the isotropic thermal factor can be also written as

$$\rho_{\varphi}(\varphi, T) = \left(\frac{1}{\pi \langle \varphi_{\text{iso}}^2 \rangle_T} \right)^{1/2} \exp \left[- \frac{(\varphi - \theta)^2}{\langle \varphi_{\text{iso}}^2 \rangle_T} \right], \quad (4)$$

where $\langle \varphi_{\text{iso}}^2 \rangle = \langle u_{\text{iso}}^2 \rangle / r^2$. At 14 K $\langle \varphi_{\text{iso}}^2 \rangle^{1/2} \approx 10^\circ$. The observed angular distribution is then a convolution product

$$P(\theta, T) = P_{\text{d}}(\theta, T) \otimes \rho_{\varphi}(\varphi - \theta, T). \quad (5)$$

Table 6

At 40 K the density distribution is best represented with a superposition of a continuous ring (see above Table 5) and a distribution of deuterons over six positions

Atom	x/a	y/b	z/c	Occupancies		
D _a	0.131(1)	0.118(1)	0.105(2)	0.26(1)		
D _b	0.0000	0.104(1)	0.148(1)	0.23(2)		
	U_{22} (Å ²)	U_{33} (Å ²)	U_{23} (Å ²)	U_{13} (Å ²)	U_{12} (Å ²)	U_{22} (Å ²)
D _a	0.012(2)	0.043(2)	0.004(2)	-0.022(2)	0.001(2)	0.012(2)
D _b	0.008(3)	0.006(2)	0.009(2)	0.0000	0.0000	0.008(3)

According to the local symmetry, the six-fold distribution is represented with two additional deuterons D_a and D_b. D_a is located at a general position in the crystal corresponding to a set of four equivalent positions. D_b is located at a special position on a mirror plane (bc) corresponding to a set of two equivalent positions. We refined the positions, the occupancies (Occ.) and the anisotropic thermal factors of D_a and D_b. The sum of the occupancies for the ring and for the 6 deuterons corresponding to a methyl group is set equal to 3.

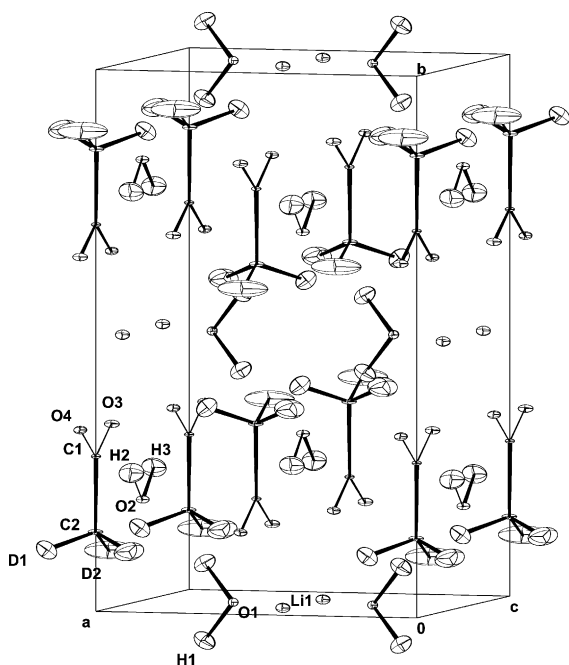


Fig. 2. Schematic view of the crystal structure of LiCOOD₃·2H₂O in the P_{man} phase at 14 K with ordered methyl groups. Thermal ellipsoids represent 50% probability for atomic positions.

At 14 K the rather sharp peaks of probability (see Fig. 3) represent well-localised deuterium atoms in a potential with the threefold symmetry. A projection onto a plane of the circular cut of the map integrated from $R = 0.9$ to $R = 1$ Å (Fig. 4)

represents the probability distribution of the angular coordinate θ . Direct comparison with angular distribution calculated for various potential barriers reveals marginal deviation of the peak positions, compared to the ideal threefold periodicity. One of the peaks is slightly broader than the others, but the integrated intensities of the three peaks are the same. These distortions are likely due to small anisotropic lattice thermal factors. Apart from these small deviations, the distribution is compatible with values for V_3 in Eq. (1) ranging from ≈ 6 to ≈ 10 meV. The calculated tunnel splitting between ≈ 60 and 20 μeV are much greater than the previously reported tunnelling frequency of 12.5 μeV [14]. We conclude that the squared wave function should be narrower than the observed distribution. At the present stage of investigation the difference can be logically attributed to broadening by convolution with librations of the molecular entities bearing the methyl groups, according to Eq. (5). However, we show below that the rotational dynamics are not properly represented with the Hamiltonian for the single methyl top, see Eq. (1) and we emphasize that rotational dynamics cannot be totally sorted out of the Fourier difference probability density.

At 300 K, the angular density distribution is almost isotropic and deuterium atoms are fully delocalised. Compared to 14 K, there is no significant increase of the width of the radial distribution. The estimated value $\langle u_r^2 \rangle_{300} \approx 0.04$ Å² is rather close to the isotropic thermal factor

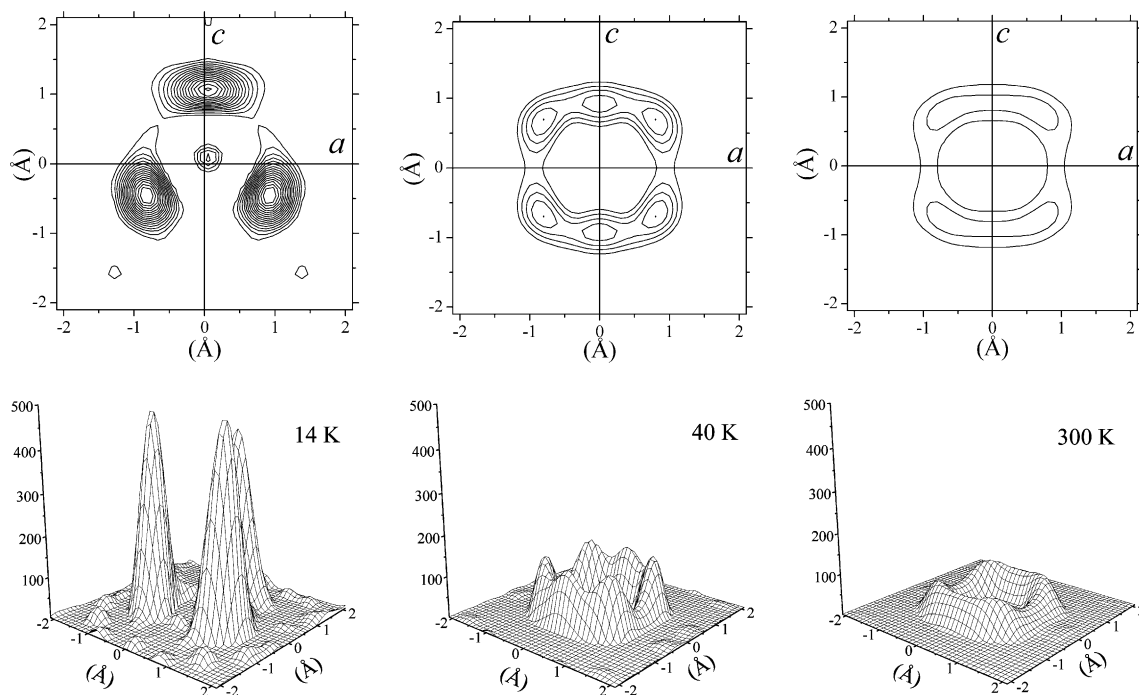


Fig. 3. Nuclear densities of the deuterium atoms of the methyl groups at 14 K (space group $Pman$), 40 and 300 K (space group $Cmmm$).

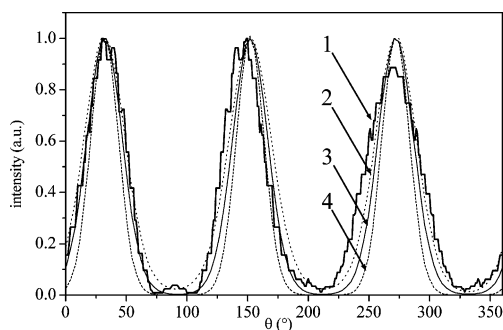


Fig. 4. Comparison of the angular probability distribution observed at 14 K with the thermally averaged probabilities calculated with wave functions for threefold potentials with various barrier heights: (1) Experimental; (2) $V_3 = 6$ meV; (3) $V_3 = 10$ meV; (4) $V_3 = 24$ meV.

($\approx 0.03 \text{ \AA}^2$, in Table 5). The square-like shape arises from the anisotropic distribution of the carbon atoms bearing the methyl groups (see C2 atoms in Table 2). The mean square displacements parallel

to the (a) direction ($\langle u_a^2 \rangle = 0.047 \text{ \AA}^2$) is much greater than that along (c) ($\langle u_c^2 \rangle = 0.028 \text{ \AA}^2$) [21].

The density distribution presented in Fig. 5 was calculated with an anisotropic distribution of the centre of mass of the methyl group over four positions located at $\pm 0.18 \text{ \AA}$ along (a) and $\pm 0.08 \text{ \AA}$ along (c). These values are within the thermal factors for C2 in Table 2. The square-like shape is clearly visible, although the dip of density along the (a) direction, clearly visible in Fig. 3, is not well represented. The crystal anisotropy is likely more pronounced than anticipated from the thermal factors.

At 40 K, the density is a superposition of delocalised ($\approx 50\%$) and localised deuterium atoms distributed over six equivalent positions ($\approx 50\%$, see Tables 5 and 6). It sounds quite unrealistic to suppose that increasing the temperature could change progressively the effective rotational potential from threefold to sixfold symmetry, and then to free rotation, whereas all other atomic coordinates remain virtually unchanged. Most

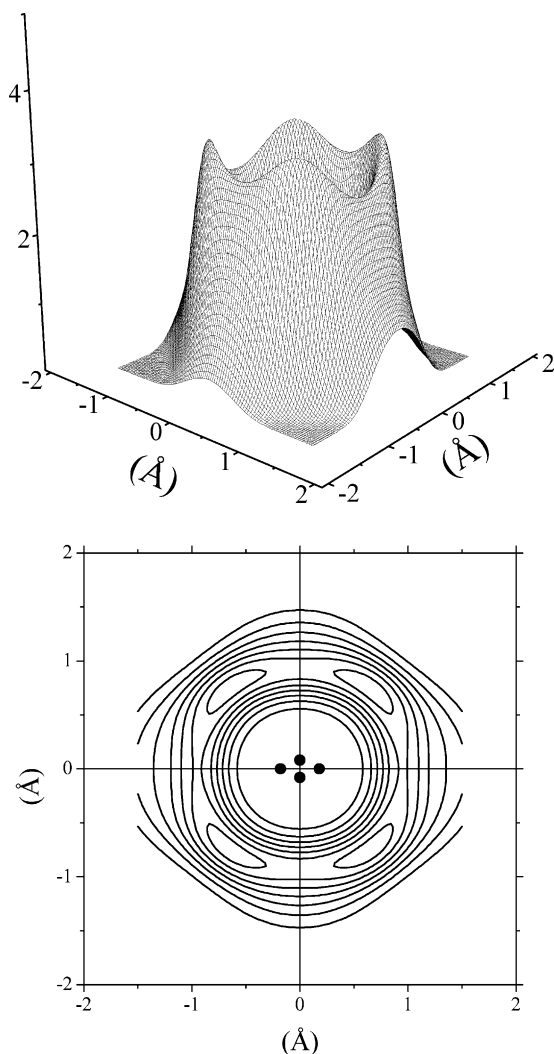


Fig. 5. Calculated isodensity contour map for deuterons at 300 K. The anisotropic density distribution of D atoms is the superposition of four isotropic distributions calculated as:

$$\rho(r) = \sum_{i=1}^2 \frac{1}{\pi(u_a)^2} \exp\left(-\frac{(r_i - r_{0a})^2}{(u_a)^2}\right) + \sum_{i=1}^2 \frac{1}{\pi(u_c)^2} \exp\left(-\frac{(r_i - r_{0c})^2}{(u_c)^2}\right).$$

The black spots located at $\pm 0.18 \text{ \AA}$ along (*a*) and $\pm 0.08 \text{ \AA}$ along (*c*) represent the centre for each distribution.

likely, the sixfold distribution arises because deuterium atoms are still partially localised at 40 K and face-to-face methyl groups are no longer indistinguishable in the *Cmmm* phase. The existence of localised deuterium atoms quite above the phase transition is direct evidence that the potential barrier does not vanish at the phase transition.

5. Quantum rotational dynamics

An intriguing paradox is that whereas the positions of heavy atoms in the unit cells are almost identical for both crystals, the probability densities for the deuterated and hydrogenated methyl groups at low temperature are extremely different (compare Fig. 3 with Fig. 8 in [22]). This spectacular difference is due to a mass effect amplified by the quantum nature of the rotational dynamics. In this section, we present dynamical models for methyl rotation and we analyse the effect of deuteration on the localisation or delocalisation of the probability density.

5.1. The single rotor

In the low-resolution limit, only a single transition at $\approx 240 \mu\text{eV}$ is distinguished in the tunnelling spectrum of Liac-h₇ and partially resolved components are ignored. Then, the threefold potential barrier in Eq. (1) is about 8 meV (see Table 7). For CD₃ the calculated tunnelling frequency is 33 μeV , quite at variance with the observed transition at 12.5 μeV [14]. The degree of delocalisation for each rotational state can be characterised with the angular mean square-root amplitude estimated as

$$\langle \theta_{n\sigma}^2 \rangle^{1/2} = \sqrt{\int_{-\pi/3}^{\pi/3} d\theta \Psi_{n\sigma}^2(\theta) \theta^2}. \quad (6)$$

Compared to the ground state, $\langle \theta_{n\sigma}^2 \rangle^{1/2}$ is a minimum for the $|0_{E\pm}\rangle$ states (see Table 7), because of the nodes in the wave functions, and then increases for higher rotational states closer to the top of the potential barrier. The maximum value of 30° corresponds to an isotropic distribution. At a low temperature (say below 20 K) the population of the rotational levels $|1_{E\pm}\rangle$ located at $\approx 4 \text{ meV}$ is negligible and the angular probability density is representative of the tunnelling states. Furthermore, the relaxation of the upper tunnelling levels at $\approx 0.240 \text{ meV}$ in Liac-h₇ is very slow and can be ignored [12,13,15]. Therefore, the observed probability density corresponds to equal populations of the three lower states: $P_d(\theta, T \approx 0) \approx [\Psi_{0A}^2(\theta) + \Psi_{0E+}^2(\theta) + \Psi_{0E-}^2(\theta)]/3$ (see Fig. 6). These densities

Table 7
Rotational energy levels for single rotors and in-phase coupled pairs

	CH ₃		CD ₃	
<i>B</i>	0.655		0.328	
<i>V</i> ₀₃	8.0		8.0	
	<i>E</i>	$\langle\theta^2\rangle^{1/2}$	<i>E</i>	$\langle\theta^2\rangle^{1/2}$
$ 0_A\rangle$	0	16	0	12
$ 0_{E\pm}\rangle$	0.240 ^a	12	0.033 ^a	9
$ 1_{E\pm}\rangle$	4.60 ^a	25	3.74 ^a	20
$ 1_A\rangle$	6.74	21	4.26	19
$ 2_A\rangle$	7.89	30	6.01	30
$ 2_{E\pm}\rangle$	11.71 ^a	–	7.41 ^a	–

Rotational constants, threefold potential barriers and energy levels are given in meV units. The angular mean amplitude $\langle\theta^2\rangle^{1/2}$ is in degrees.

^a Twofold degeneracy.

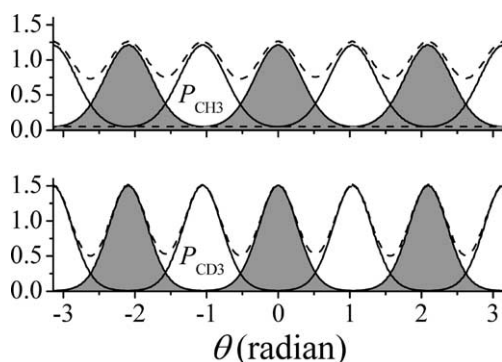


Fig. 6. Calculated angular probabilities at 14 K for single CH₃ and CD₃ rotors in the threefold potential function $V_{03} = 8.0$ meV. Energy levels are given in Table 7. The distributions for a methyl group (solid line with filled area), for a staggered methyl group (solid line) and for a pair of staggered rotors (dash line) are superimposed.

can be decomposed into a constant part for full delocalisation ($\approx 4\%$ for CH₃ and less than 1% for CD₃) and a threefold function for the localised distribution. Therefore, CH₃ and CD₃ rotors should be markedly localised at low temperature and their angular density probabilities should be very similar.

However, it could be suspected that direct comparison of the density calculated for a single CD₃ rotor with the Fourier difference is relevant only in the ordered phase (*Pman*), whereas the

observed density in the disordered phase (*Cmmm*) with the sixfold symmetry should be represented with a superposition of the density for two face-to-face methyl groups with the staggered configuration. The dash lines in Fig. 6 show that the calculated probability for staggered CH₃ groups remains markedly localised and this is in conflict with the Fourier difference previously determined for Liac-h₇ at 5 K [7]. Even if we have ignored possible smoothing of the angular distribution due to isotropic thermal factors, this model can be safely rejected.

The delocalisation should increase with temperature according to, approximately, a first order law with an activation energy of ≈ 4 meV corresponding to upper rotational levels for both hydrogenated and deuterated methyl groups (see Table 7). At 40 K, for example, the thermal population of upper rotational states should be rather modest and the estimated proportion of delocalised atoms ($\approx 25\%$) should be very similar for both systems. We conclude that the single rotor model cannot account for the markedly different temperature effects observed for the CH₃ and CD₃ derivatives at low temperature.

5.2. The coupled pair

Coupled pairs with parallel axes of rotation offer a more realistic view of the rotational dynamics. These dynamics were previously represented, Clough et al., with the Hamiltonian depending on the angular coordinates θ_1 and θ_2 for each rotor [12,14,23]:

$$H_2 = -B \left(\frac{\partial^2}{\partial \theta_1^2} + \frac{\partial^2}{\partial \theta_2^2} \right) + \frac{V_{03}}{2} \cos 3\theta_1 + \frac{V_{03}}{2} \cos 3\theta_2 + \frac{W_{12}}{2} \cos 3(\theta_1 - \theta_2). \quad (7)$$

Each top experiences the same on-site potential and the coupling depends only on the phase difference for the two rotors. In contrast to the textbook case of two coupled harmonic oscillators, this Hamiltonian cannot be diagonalised by simple transformation of the internal coordinates into normal coordinates [24]. Moreover, numerical calculations of the eigenstates requires rather large

basis sets (say $2N$) for each rotor. The level of accuracy depends on N and the higher the potential barrier is, the larger N should be. As we want to understand the rotational dynamics up to room temperature we must calculate at least 10 eigenstates and good accuracy in one dimension is obtained with $N \sim 40$ (see Section 2). For the coupled pair, the two angular coordinates must be treated simultaneously because symmetric and antisymmetric states are no longer separate. Therefore, in order to obtain the same level of accuracy as for the single top, the matrix should have dimension $(2N \times 2N)^2 : 6400 \times 6400$. Diagonalization of such large matrices is not routinely feasible. Furthermore, as symmetric and antisymmetric states are mixed, the interpretation of the calculated energy level scheme is tedious in the absence of theoretical rules. Early calculations carried out with very limited basis sets [12] were certainly lacking of accuracy and deserve some reservations. Even with more refined computational recipes, limited basis sets yield large inaccuracy for rotational levels above the tunnelling states [25].

The huge matrix size and the resulting lack of accuracy arise because the basis sets do not account for centre of symmetry for pairs of methyl groups in lithium acetate. The symmetry of the eigenstates was determined in the particular limit of uncoupled free rotors, $V_{03} = W_{12} = 0$ [12]. Then, using the same notation as these authors, the level scheme is composed of the ground state ($|A_1A_2\rangle$ at $E = 0$), two degenerate first excited states corresponding to the transfer of one quantum to one of the two tops ($|E_1^\pm A_2\rangle$ and $|A_1 E_2^\pm\rangle$ at $E = B$) and higher excited states corresponding to the transfer of one quantum to each top, either in-phase or anti-phase ($|E_1^\pm E_2^\pm\rangle$ and $|E_1^\pm E_2^\mp\rangle$ at $E = 2B$). The energy level scheme for non-zero-potential terms was obtained by continuation of the zero-potential limit. It was speculated that $|E_1^\pm A_2\rangle$ and $|A_1 E_2^\pm\rangle$ states should remain degenerate in all cases and the coupling merely split $|E_1^\pm E_2^\pm\rangle$ and $|E_1^\pm E_2^\mp\rangle$. However, two coupled rotors are, by definition, indistinguishable. Consequently, $|E_1^\pm A_2\rangle$ and $|A_1 E_2^\pm\rangle$ cannot be eigenstates of Eq. (7) for straightforward symmetry consideration. This scheme is seriously in error and leads to misinter-

pretation of the spectra. The numerical values ($V_{03} \approx 7.6$ meV and $W_{12} \approx -17.0$ meV) derived from the INS spectra [14] are in conflict with the crystal structure. The on-site potential barrier, quite similar to that obtained with the single rotor model, is unrealistic with regard to the observed probability density distribution (see above Section 5.1). Moreover, among the four transitions anticipated, three of them are hot transitions and they should vanish at a low temperature, at thermal equilibrium. However, experiments [13] did not provide any clear-cut confirmation.

A more focused view of the dynamics was sought with the INS spectra of mixtures of CH_3 and CD_3 derivatives [14]. The physical and chemical differences for the two analogues are negligible, compared to intermolecular interactions in the crystal, and mixtures are statistical distributions of pairs. If x and $(1-x)$ are the relative concentrations of CD_3 and CH_3 , respectively, then the relative concentrations of pairs $\text{CH}_3\text{-CH}_3$, $\text{CH}_3\text{-CD}_3$ and $\text{CD}_3\text{-CD}_3$ are $(1-x)^2$, $2x(1-x)$ and x^2 , respectively.

Owing to the great difference of tunnelling frequencies for CH_3 and CD_3 rotors, the mixed pairs should be totally decoupled and the splitting arising from the relative rotation of the two tops, namely $|E_H^\pm E_D^\pm\rangle$ and $|E_H^\pm E_D^\mp\rangle$, can be ignored. The spectrum is composed of virtually degenerate transitions: $|A_H\rangle \rightarrow |E_H\rangle$ and $|A_D\rangle \rightarrow |E_D\rangle$. If there were no change of the effective potential upon isotope substitution, the frequency of a decoupled rotor should be at the barycentre of the spectral profile for the coupled pair.

The transitions reported for mixtures containing small concentrations of CH_3 (from 5% to 20%) in CD_3 environment were decomposed into a main peak at 130 μeV and a weak shoulder at 180 μeV attributed to $\text{CH}_3\text{-CD}_3$ and $\text{CH}_3\text{-CH}_3$ pairs, respectively [14]. For an increasing concentration of CH_3 , the band intensity at 130 μeV decreases, that at 180 μeV increases to a maximum value for a concentration of $\approx 66\%$ and then decreases whilst new features appear at ≈ 250 μeV , due to fully hydrogenated pairs. Therefore, there are at least three bands instead of the two anticipated. The extra band was attributed to $\text{CH}_3\text{-CH}_3$ pairs surrounded by deuterated rotors, which increase the

effective potential barrier. The band at $\approx 250 \mu\text{eV}$ in the fully hydrogenated crystal was thus supposed to be shifted to $\approx 180 \mu\text{eV}$. However, each pair has four nearest neighbours in the crystal. Therefore, different effective potentials should occur for different concentration in CD_3 groups and give a statistical distribution of four transitions between 250 and 180 μeV . Apparently, these transitions were not resolved and a smooth frequency shift should be observed, rather than changes of relative intensities for separate transitions at fixed frequencies. With hindsight, we understand that the interpretation was hampered by the different crystal structures for the two analogues. This complication was totally unforeseeable at that time.

5.3. Symmetry adapted coordinates

We propose a more rigorous analysis of the dynamics of coupled pairs based on the crystal structure showing centrosymmetric pairs of face-to-face methyl groups. The dynamics are better represented with symmetry-adapted angular coordinates corresponding to in-phase $\theta_i = (\theta_1 + \theta_2)/2$ and anti-phase $\theta_a = (\theta_1 - \theta_2)/2$ rotation. In contrast, again, to the pair of coupled harmonic oscillators, the choice of rotational coordinates is imposed by the periodicity of the rotors. The coordinates must be adapted to the threefold and sixfold periodicities for in-phase and anti-phase rotation. Any alternative choice should give a dramatically different, and physically irrelevant, energy level scheme. The Hamiltonian for a centrosymmetric pair of coupled methyl groups is then rewritten as

$$H_{2ia} = H_{2i}(\theta_i) + H_{2a}(\theta_a), \quad (8)$$

with

$$H_{2i}(\theta_i) = -\frac{B}{2} \frac{\partial^2}{\partial \theta_i^2} + \frac{V_{3i}}{2} \cos 3\theta_i, \quad (9)$$

$$H_{2a}(\theta_a) = -\frac{B}{2} \frac{\partial^2}{\partial \theta_a^2} + \frac{V_{3a}}{2} \cos 3\theta_a + \frac{W_{12a}}{2} \cos 6\theta_a.$$

For in-phase rotation the coupling term vanishes and the dynamics is that of a single rotor

with moment of inertia $2I_r$ experiencing a threefold potential. If the coupling potential is strongly attractive, the pair is in the eclipsed conformation and the effective potential is $V_{3i} \approx 2V_{03}$. Alternatively, if the staggered configuration is favoured by a repulsive coupling potential, the effective sixfold potential should be very weak and nearly free rotation is anticipated. Finally, for anti-phase rotation, the effective potential comprises contributions from V_{3a} and W_{12} .

An important consequence of the symmetry-adapted coordinates is that the rotational constant is divided by a factor 2 compared to the single rotor. The maximum frequency for free rotation is now in the range 325–350 μeV for a pair of CH_3 and 162–175 μeV for the deuterated analogue. Therefore, transitions observed at $\approx 270 \mu\text{eV}$ may effectively correspond to pairs of CH_3 groups rotating almost freely [10].

The energy level scheme in the tunnelling frequency range (see Fig. 7) is composed of one tunnelling state for in-phase rotation in a threefold potential ($|0_{E\pm}\rangle_i$) and three states for anti-phase rotation in a sixfold potential ($|0_{E\pm}\rangle_a$, $|1_{E\pm}\rangle_a$

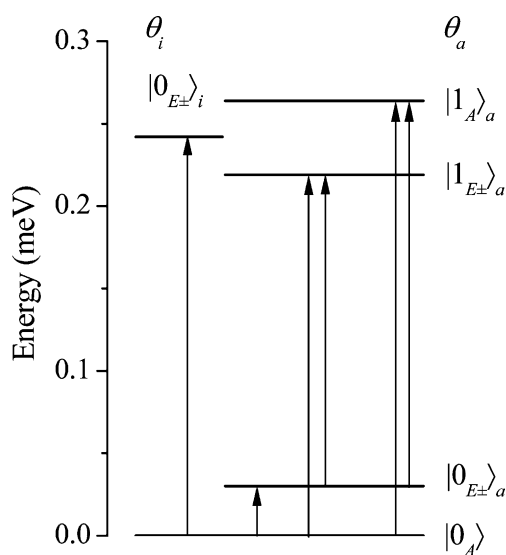
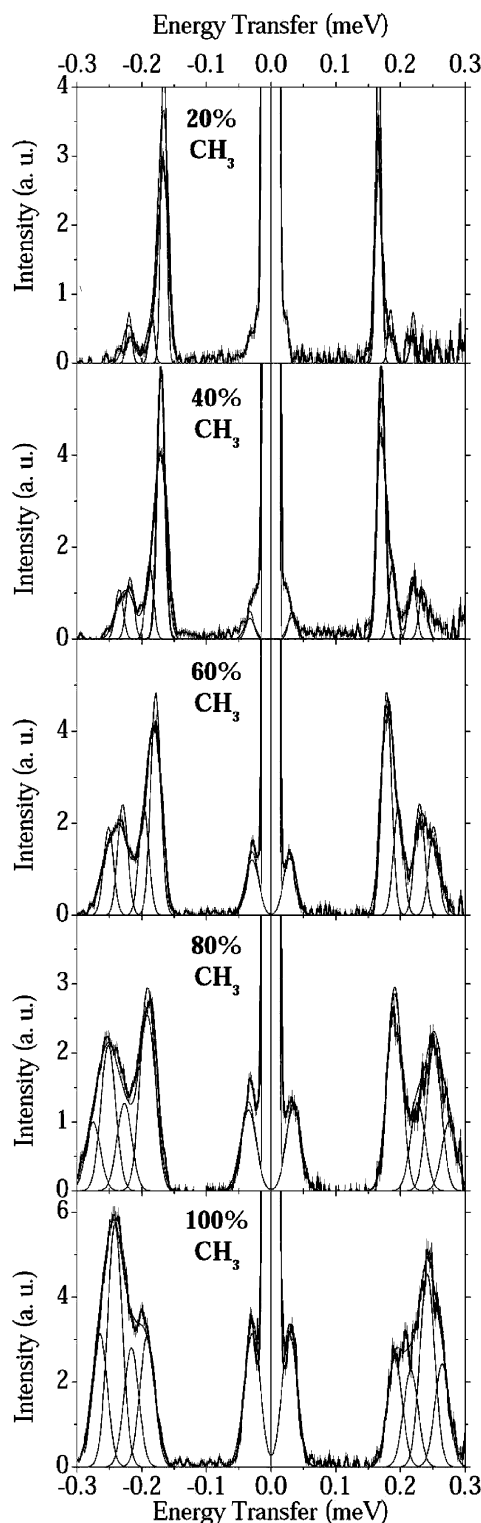


Fig. 7. Qualitative energy level scheme for a centrosymmetric pair of coupled rotors with fixed parallel axes. The angular coordinates θ_i and θ_a correspond to in-phase and anti-phase rotation of the tops. The relative position of the $|0_{E\pm}\rangle_i$ level with respect to the others is inspired by the INS spectra shown in Fig. 8.



and $|1_A\rangle_a$). There are four fundamental transitions ($|0_A\rangle \rightarrow |0_{E\pm}\rangle_i$, $|0_A\rangle \rightarrow |0_{E\pm}\rangle_a$, $|0_A\rangle \rightarrow |1_{E\pm}\rangle_a$, $|0_A\rangle \rightarrow |1_A\rangle_a$) and two “hot” transitions ($|0_{E\pm}\rangle_a \rightarrow |1_{E\pm}\rangle_a$, $|0_{E\pm}\rangle_a \rightarrow |1_A\rangle_a$). The assignment of the band at $\approx 30 \mu\text{eV}$ to the $|0_A\rangle \rightarrow |0_{E\pm}\rangle_a$ transition is unambiguous. We anticipate five bands in the $270 \mu\text{eV}$ range whereas only three bands have been reported previously. However, the bandwidth of $\approx 21 \mu\text{eV}$ for each component [14] is similar to the difference between fundamental and hot transitions. Therefore, if we suppose that hot transitions were not resolved from their parent bands, then the three bands correspond to transitions to $|0_{E\pm}\rangle_i$, $|1_{E\pm}\rangle_a$ and $|1_A\rangle_a$, respectively.

5.4. Isotope mixtures

The INS spectra of mixtures of CH_3 and CH_2D derivatives (see Fig. 8) give more details. We conjecture that the change of the effective potential due to the mass is minimized and any phase transition analogous to that observed for the CD_3 derivative is much less likely for CH_2D . A further advantage is that all mixed pairs have significant INS cross-sections and the corresponding tunneling transitions should be observed. However, owing to the different pair potentials for H...H, H...D and D...D atoms [26] anti-phase tunnelling should be cancelled for $\text{CH}_2\text{D}-\text{CH}_2\text{D}$ pairs. Otherwise, we tentatively assume that partial deuteration does not breakdown the threefold periodicity of the effective potentials for in-phase rotation.

The INS bandwidths are effectively diminished by a factor of ≈ 3 in the most diluted isotope mixture compared to the fully hydrogenated crystal (see Table 8). Due to the increased resolution, the evolution of the spectra with the relative concentration yields at least four components located between 150 and 300 μeV in Liac-h₇, instead of three reported previously [12–14]. These bands

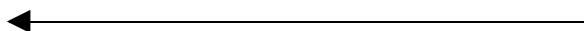


Fig. 8. INS spectra of mixtures of LiCH_3COO , $2\text{H}_2\text{O}$ and LiCH_2DCOO , $2\text{H}_2\text{O}$ at 2 K. The signal in the range of negative energy transfer (neutron energy gain) was deconvoluted according to the spectrometer resolution function and to the bandwidth observed in the range of positive energy transfer (neutron energy loss).

Table 8

Band decomposition of mixtures containing various concentrations of the fully hydrogenated lithium acetate Liac-h₇ in the CH₂D analogue

Liac-h ₇	FWHH		1	2	3	4	5
20%	8	Frequency	220	–	185	166	–
		Area	11	–	12	77	–
40%	13	Frequency	237	219	187	171	32
		Area	9	13	14	57	7
60%	19	Frequency	255	232	202	180	29
		Area	12	21	12	42	12
80%	22	Frequency	276	251	225	191	31
		Area	10	26	13	32	19
100%	22	Frequency	264	241	216	191	29
		Area	17	31	16	17	19

Band frequencies and full width at half height (FWHH) are in μeV units. The relative band areas are in % of the total band intensity for each spectrum.

are compatible with the assignment scheme presented in Fig. 7. The assignment of the band at $\approx 30 \mu\text{eV}$ to the $|0_A\rangle \rightarrow |0_{E\pm}\rangle_a$ transition due to out-of-phase rotation of CH₃–CH₃ pairs is confirmed. This band has no visible analogue for CH₂D–CH₂D pairs. At a low concentration in CH₃ (20%) the most intense band at 166 μeV and the weaker band at 185 μeV can be attributed to in-phase rotation ($|0_A\rangle \rightarrow |0_{E\pm}\rangle_i$) of CH₂D–CH₂D and CH₃–CH₂D pairs, respectively. The weak transition at 220 μeV is tentatively assigned to anti-phase tunnelling of CH₃–CH₂D pairs. For increasing concentration in CH₃ the band intensity around 170 μeV decreases whilst the frequency shifts smoothly upwards to 191 μeV for 100% of

CH₃ rotors. Presumably, transitions due to CH₂D–CH₂D and CH₃–CH₂D pairs are not resolved. We extrapolate to 164 and 185 μeV the frequency for in-phase tunnelling of CH₂D–CH₂D and CH₃–CH₂D pairs, respectively.

With the unambiguous assignment of the in-phase tunnelling for CH₃–CD₃ (130 μeV) and CH₂D–CH₂D (164 μeV), we assign the transition at 241 μeV in Liac-h₇ to in-phase tunnelling of CH₃–CH₃ entities ($|0_A\rangle \rightarrow |0_{E\pm}\rangle_i$). The estimated values of V_{3i} for each pair are given in Table 9. For pairs containing H atoms, we obtain an averaged value of $V_{3i} = (1.82 \pm 0.15) \text{ meV}$. This rather modest dispersion of $\approx 10\%$ may arise from experimental errors, band shape analysis and small

Table 9

Rotational energy levels for in-phase coupled pairs

	CH ₃ –CH ₃		CH ₃ –CH ₂ D		CH ₂ D–CH ₂ D		CH ₃ –CD ₃		CD ₃ –CD ₃	
B	0.328		0.281		0.246		0.219		0.164	
V_{3i}	1.90		1.96		1.67		1.74		4.5	
	E	$\langle\theta^2\rangle^{1/2}$	E	$\langle\theta^2\rangle^{1/2}$	E	$\langle\theta^2\rangle^{1/2}$	E	$\langle\theta^2\rangle^{1/2}$	E	$\langle\theta^2\rangle^{1/2}$
$ 0_A\rangle$	0	21	0	19	0	19	0	18	0	11
$ 0_{E\pm}\rangle$	<i>0.241^a</i>	16	<i>0.185^a</i>	15	<i>0.164^a</i>	15	<i>0.131^{a,b}</i>	15	<i>0.012^{a,b}</i>	8
$ 1_{E\pm}\rangle$	1.61 ^a	25	1.48 ^a	25	1.28 ^a	25	1.22 ^a	25	2.08 ^a	19
$ 1_A\rangle$	3.07	22	2.68	22	2.34	22	2.11	21	2.29	19
$ 2_A\rangle$	3.22	29	2.86	30	2.49	30	2.29	30	3.37	30
$ 2_{E\pm}\rangle$	5.42 ^a	–	4.71 ^a	–	4.11 ^a	–	3.70 ^a	–	4.02 ^a	–

Rotational constants, threefold potential barriers and energy levels are given in meV units. The angular mean amplitude $\langle\theta^2\rangle^{1/2}$ is given in degrees. The observed tunnelling transitions are italicised.

^a Twofold degeneracy.

^b From [14].

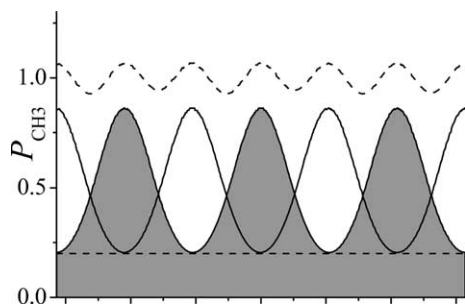


Fig. 9. Calculated angular probabilities at 14 K for the CH_3 – CH_3 pair in a threefold potential barrier $V_{3i} = 1.92$ meV. Energy levels are presented in Table 8. The distributions for a methyl group (solid line with filled area), for a staggered methyl group (solid line) and for a pair of staggered rotors (dash line) are superimposed.

variations of the effective potential with the mass. However, there is no simple correlation between the potential barrier and the rotational constant. The calculated density probability for CH_3 pairs in the disordered phase is now virtually isotropic (see Fig. 9, dash line), in agreement with the Fourier difference. On the other hand, the potential barrier of ≈ 4.5 meV for CD_3 – CD_3 pair confirms a dramatic change upon full deuteration.

We have virtually no information for anti-phase rotation of the deuterated species. For CH_3 – CH_3 pairs, we assign the doublet at 191 and 216 μeV to $|0_{E\pm}\rangle_a \rightarrow |1_{E\pm}\rangle_a$ and $|0_A\rangle \rightarrow |1_{E\pm}\rangle_a$, respectively. The splitting of 25 μeV compares to the $|0_A\rangle \rightarrow |0_{E\pm}\rangle_a$ transition observed at 29 μeV . Similarly, we assign the component at 264 μeV to $|0_A\rangle \rightarrow |1_A\rangle_a$ and we suppose that the companion transition $|0_{E\pm}\rangle_a \rightarrow |1_A\rangle_a$ anticipated at 235 μeV is a part of the main component at 241 μeV . Here we also suppose that all transitions have about the same intensity. The best fit is obtained with the effective potential terms in Eq. (9) $V_{3a} = 0.19$ meV and $W_{12a} = 31.64$ meV.

6. Coupling between pairs and phase transition mechanism

Inspection of the arrangement of acetate entities in the (a, b) plane reveals a network of methyl groups in 2D with honeycomb-like structure (see Fig. 10). According to the methyl–methyl distances

of 3.3 Å within pairs and 4.2 Å for next nearest neighbours, the coupling term between adjacent methyl groups along the a direction should be weaker than the intra-pair coupling potential, but, nevertheless, significant. On the other hand, interactions between molecules in different (a, b) planes separated by ≈ 6.6 Å are certainly much weaker and can be ignored. Therefore, collective effects due to coupling between pairs should occur essentially in 2D.

For anti-phase dynamics, coupling between pairs is certainly negligible compared to the high sixfold potential barrier. Moreover, this dynamics does not contribute to the ordering/disordering mechanism.

For in-phase rotation, the on-site potential is rather weak and coupling between pairs can be on the same order of magnitude [15]. We assume that the phase transition arises from interactions between pairs of methyl groups. Each pair interacts with the four nearest neighbour methyl groups in the same (a, b) plane. The Hamiltonian can be written as

$$H_{ci} = -\frac{B}{2} \frac{\partial^2}{\partial \theta_i^2} + \frac{V_{03i}}{2} (1 - \cos 3\theta_i) + \sum_{j=1}^4 \frac{V_{ci}}{2} [1 - \cos 3(\theta_{ij} - \theta_i)]. \quad (10)$$

In the ordered crystal structure at a low temperature the coupling potential is a minimum for $\theta_{ij} = \theta_i$. It can be expanded as

$$\sum_{j=1}^4 \frac{V_{ci}}{2} (1 - \cos 3\theta_i \cos 3\theta_{ij} - \sin 3\theta_i \sin 3\theta_{ij}). \quad (11)$$

In the weak-coupling (order/disorder) regime, there is no correlation between the angular coordinate of the pair (θ_i) and those of the neighbours (θ_{ij}). Average over the distribution of phase differences cancels the $\sin 3\theta_{ij}$ term and the effective potential experienced by a pair can be written as

$$\frac{V_{3i}^{\text{eff}}}{2} [1 - \cos 3\theta_i] \approx \frac{V_{03i} + 4V_{ci} \cos[3\bar{\theta}(T)]}{2} [1 - \cos 3\theta_i]. \quad (12)$$

Here, $\bar{\theta}(T) = \langle \theta_{ij}^2(T) \rangle^{1/2} = \langle \theta_i^2(T) \rangle^{1/2}$ (see Eq. (6)) is the mean value of the angular coordinate depending on the temperature. At a low tempera-

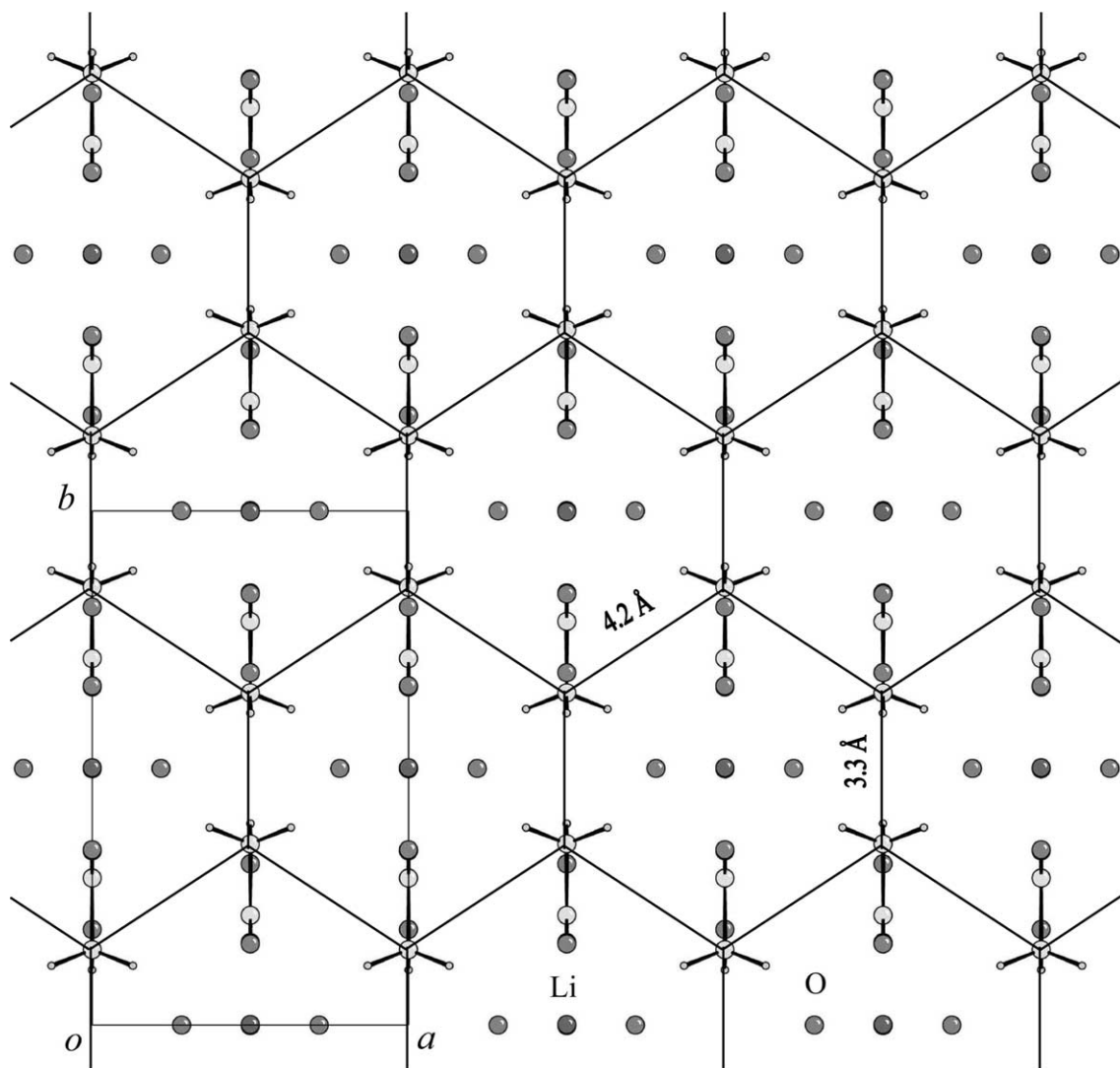


Fig. 10. Schematic representation of the honeycomb-like arrangement of the methyl rotors in the (a, b) plane of the ordered structure at 14 K. Solid lines are guides for the eyes. For the sake of clarity the protons of the water molecules are not shown.

ture, $\bar{\theta}_H \approx 17.5^\circ$ and $\bar{\theta}_D \approx 9^\circ$ for CH_3 and CD_3 pairs, respectively (after Table 9). Then, assuming that the increase of the effective potential barrier upon methyl deuteration is due to the change of the mean angular amplitude, we obtain from Eq. (12) $4V_{ci} \approx 9.2$ meV and $V_{03i} \approx -3.7$ meV.

The effective potential in Eq. (12) vanishes for $\bar{\theta}_0 \approx 22^\circ$. However, in the quantum regime this value is not critical since the delocalisation of the wave function survives for non-vanishing potential

barriers (see Fig. 9). The full delocalisation of the CH_3 group orientation evidenced by the neutron diffraction technique, even at a very low temperature, confirms that the value $\bar{\theta}_H \approx 17.5^\circ$ is sufficiently close to $\bar{\theta}_0$ to prevent long-range correlation. As this value of $\bar{\theta}_H$ cannot be further decreased, for example upon cooling the sample, we do not anticipate any ordering of the methyl groups at any temperature. Conversely, in the classical regime, ordering of the methyl groups should occur at

sufficiently low temperature for a non-vanishing potential barrier. The crystal structure of Liac-h₇ at low temperature is directly related to the quantum nature of the methyl rotors.

The phase transition for the methyl-deuterated analogue arises because quantum effects are much less pronounced for CD₃ rotors. At low temperature $\bar{\theta}_D \approx 9^\circ$ (Table 9), the effective potential barrier is increased and long-range ordering takes place. As the temperature is increased, the rotational levels at ≈ 2 meV (see Table 9) are populated; $\bar{\theta}_D$ increases whilst the effective potential barrier decreases. As a very rough approximation the increase of $\bar{\theta}_D$ should follow a first order law with activation energy of ≈ 2 meV and the phase transition could take place when the thermal bath has a similar energy (namely, ≈ 22 K). This temperature is rather close to the temperature of 17.5 K measured for the phase transition. In fact, as the temperature is increased, the effective potential barrier decreases; the energy of the first rotational level also decreases; the population of the rotational states increases more rapidly than anticipated with the first order law. The qualitative agreement with experiments is quite satisfactory regarding approximations in calculations. It is worth emphasizing that the low temperature for the phase transition is a further confirmation of the diminishing of the rotational constant for coupled pairs, compared to single rotors. Alternative dynamical models can be rejected confidently. They would give activation energy of ≈ 4 meV (see Table 7) and the phase transition, if any, would occur at a much higher temperature.

Eqs. (10)–(12) account for the phase transition but more detailed modelling of the rotational statistics should be necessary to account for the co-existence of ordered and disordered domains suggested by the probability density at 40 K (see Fig. 3).

7. Discussion

7.1. Coupling with phonons

Coupling between angular coordinates and extended lattice modes (phonon coordinates x_k)

was proposed to account for the variation of the effective potential upon deuteration and temperature (phonon mediated coupling) [14,27,28]. Phonons were represented with harmonic oscillators but without any further consideration to the extended nature of these excitations. The model of rotational tunnelling coupled with translation of the centre of mass is very similar in spirit [7]. This model deserves critical comments. Firstly, there is no optical phonon in the tunnelling region. In a crystal like lithium acetate the lowest phonon frequency is one order of magnitude greater than the highest tunnelling transition. Therefore, mixing tunnelling states with optical phonons would require very large coupling terms. This is physically unlikely. (As opposed to this, coupling between phonons and methyl rotational states is quite possible [29].) Secondly, coupled tunnelling-phonon states should not be amenable to isolated rotors or pairs. They should be regarded as extended tunnelling states with some dispersion. Thirdly, coupling with phonons should increase the effective moment of inertia and dramatically change the effective potential barrier. However, the effective rotational constant cannot be set to an arbitrary value since it must be greater than the highest tunnelling frequency. For Liac-h₇ the upper limit of ≈ 300 μ eV imposes that coupled pairs are virtually uncoupled to phonons. Alternatively, coupling with phonon would impose the single rotor model and only one tunnelling band should be observed. This must be rejected regarding the complexity of the tunnelling spectra.

The strong limitation of the phonon mediated coupling model does not mean that there is no influence of the lattice dynamics on rotational dynamics. The methyl groups linked to the molecular frame ride the lattice modes. These vibrations are included in the thermal factors obtained from diffraction measurements (see Tables 1–3). They partially determine the effective rotational potential terms by averaging the crystal field over the fast zero-point motions. The thermal factors for heavy atoms are very similar for all isotope derivatives and these values are not significantly affected by the phase transition (compare values in Tables 3 and 4). They cannot account for the

marked changes of the effective potential upon methyl deuteration.

7.2. Local versus collective rotational dynamics

Comparison of the methyl dynamics in 4-methylpyridine [16,26,29,30] and lithium acetate shed a new light on the interplay of structure and dynamics. From the viewpoint of the crystal structures, these two systems have in common pairs of face-to-face methyl groups with rather short distances of ≈ 3.5 and 3.3 Å, respectively. The two systems have also in common rather short distances between pairs. In the 4-methylpyridine crystal, the unit cell is tetragonal $I4_1/a$ and the rotational axis of a pair is parallel to (*c*). Methyl groups form infinite chains parallel to (*a*) and (*b*) with a distance of ≈ 4 Å between nearest neighbours. In the lithium acetate crystal infinite chains parallel to the (*a*) direction and with a distance of ≈ 4.2 Å between nearest neighbours can be seen (see Figs. 1, 2 and 10). It is quite remarkable that such great similarities of the crystal structures may give rise to extremely different rotational dynamics.

In the 4-methylpyridine crystal each methyl group in a pair belongs to orthogonal chains parallel to the (*a*) or (*b*) axes, respectively. The C_2 site symmetry imposes disordering of the methyl groups and the angular density probability is virtually isotropic, even at 10 K [31]. There is no centre of symmetry for the pairs and methyl groups cannot perform concerted rotation. The tunnelling transitions occur in the 460–540 μeV region, rather close to the upper limit for a single methyl group. This is unquestionable evidence for single rotors uncoupled to phonons. The collective nature of the rotational dynamics is evidenced by a continuous frequency shift ($\Delta\nu/\nu$ up to 30%) in isotope mixtures of fully hydrogenated and fully deuterated molecules and temperature effects, which seem to annihilate frequency shifts due to deuteration [16,30]. Collective dynamics are represented with the quantum sine-Gordon theory for isolated chains of coupled rotors in 1D. The on-site potential with the threefold symmetry is ≈ 3.7 meV and the coupling term between nearest neighbours is ≈ 5.5 meV. Comparison with lithium acetate emphasizes the cancellation of the large

coupling potential within pairs owing to the crystal symmetry.

In contrast to 4-methylpyridine, the arrangement of the methyl groups in the lithium acetate crystal has a marked 2D character (see Fig. 10) and the centrosymmetric pairs can perform combined rotation. The coupling potential within pairs is by far much greater than any other methyl–methyl interaction in the crystal.

8. Conclusions

The lithium acetate crystal is a prototype system to investigate the interplay of the crystal structure and rotational dynamics of nearly free quantum rotors. For the methyl-deuterated salt crystallised with H_2O molecules we have observed a phase transition at (17.5 ± 0.5) K. The disordered methyl groups in the high temperature phase ($Cmmm$) become ordered at low temperature ($Pnma$), whereas all other atomic positions remain virtually unchanged. The same transition occurs for the fully deuterated analogue, but not for the fully hydrogenated system. We conclude that the transition is due to the increased mass of the methyl groups upon deuteration whereas the role of water molecules and other atoms is marginal.

The maps of probability density in the rotational plane of the methyl groups provide graphic views of the localisation/delocalisation of the D atoms at various temperatures. These maps are convolutions of the distribution of the angular coordinate arising from rotational dynamics with distributions due to internal modes of the methyl groups and with the lattice thermal factors.

The maps shed a new light onto the quantum rotational dynamics. Firstly, full delocalisation of the density map for hydrogen atoms in Liac- h_7 at low temperature [7] is in conflict with previous estimates of the effective potential barrier [12,14]. Secondly, the effective potential barrier at a low temperature is increased by methyl deuteration. Thirdly, the barrier for CD_3 rotation is not cancelled at the transition to the disordered phase. Both delocalised and localised atoms coexist over a large temperature range. All these observations

are explained with the dynamics of coupled pairs of methyl groups.

The rotational dynamics of centrosymmetric pairs of face-to-face methyl groups is represented with symmetry-adapted coordinates corresponding to in-phase and anti-phase rotation. The Hamiltonian split into two independent dynamical systems corresponding to single rotors whose moments of inertia are twice that for a single methyl group. It is then straightforward to account for the tunnelling transitions with nearly free rotors. A new assignment scheme is established for the tunnelling states.

In order to account for the phase transition, we consider methyl–methyl interaction between nearest neighbour pairs in the (*a*, *b*) planes. The effective potential for in-phase rotation is the sum of two opposite contributions that depend on mass and temperature via the mean root-square amplitude of the angular coordinate. Low potential barriers along with low rotational constants account for the phase transition induced by deuteration of the methyl groups. Alternative models for the rotational constant can be safely rejected.

This work demonstrates that thorough experimental studies with the complementary neutron diffraction and INS tunnelling techniques may reveal the otherwise hidden interplay of crystal structures and quantum rotational dynamics, at levels of accuracy and physical understanding far beyond what can be obtained with the most advanced computational methods of quantum chemistry.

Acknowledgements

We thank N. Ratovélomanana from LADIR for sample preparation and J. Godard from Parc d'Orsay (Orsay, France) for growing single crystals.

References

- [1] M. Prager, H. Heidemann, *Chem. Rev.* 97 (1997) 2933.
- [2] A.J. Dianoux, G. Lander (Eds.), *Neutron Data Booklet*, Institut Laue-Langevin, Neutrons for Science, Grenoble, 2002.
- [3] W. Press, A. Kollmar, *Solid State Commun.* 17 (1975) 405.
- [4] B. Alefeld, A. Kollmar, B.A. Dasannacharya, *J. Chem. Phys.* 63 (1975) 4415.
- [5] W. Press, *Springer Tracts in Modern Physics*, vol. 92, Springer, Berlin, 1981.
- [6] M. Neumann, M.R. Johnson, *J. Chem. Phys.* 215 (1997) 253.
- [7] P. Schiebel, G.J. Kearley, M.R. Johnson, *J. Chem. Phys.* 108 (1998) 2375.
- [8] J.L. Galigné, M. Mouvet, J. Falgouttes, *Acta Cryst. B* 26 (1970) 368.
- [9] G.J. Kearley, B. Nicolai, P.G. Radaelli, F. Fillaux, *J. Solid State Chem.* 126 (1996) 184.
- [10] P.S. Allen, P. Branson, *J. Phys. C: Solid State Phys.* 11 (1978) L121.
- [11] S. Clough, A. Heidemann, M.N.J. Paley, *J. Phys. C: Solid State Phys.* 13 (1980) 4009.
- [12] S. Clough, A. Heidemann, A.H. Horsewill, M.N.J. Paley, *Z. Phys. B* 55 (1984) 1.
- [13] A. Heidemann, K.J. Abed, C.J. Barker, S. Clough, *Z. Phys. B* 66 (1987) 355.
- [14] A. Heidemann, H. Fredrich, E. Günther, W. Häusler, *Z. Phys. B* 76 (1989) 335.
- [15] F. Fillaux, G.J. Kearley, C.J. Carlile, *Physica B* 226 (1996) 241.
- [16] F. Fillaux, C.J. Carlile, *Phys. Rev. B* 42 (1990) 5990.
- [17] D.J. Watkin, C.K. Prout, J.R. Carruthers, P.W. Betteridge, R.I. Cooper, *CRYSTALS Issue 11*, Chemical Crystallography Laboratory, University of Oxford, Oxford, UK, 1999.
- [18] V.F. Sears, *Neutron News* 3 (1992) 26.
- [19] J.D. Lewis, T.B. Malloy Jr., T.H. Chao, J. Laane, *J. Mol. Struct.* 12 (1972) 427.
- [20] J.R. Durig, S.M. Craven, W.C. Harris, *Vibrational Spectra and Structure*, Marcel Dekker, New York, 1972.
- [21] B. Nicolai, G.J. Kearley, A. Cousson, W. Paulus, F. Fillaux, F. Gentner, L. Schröder, D. Watkin, *Acta Cryst. B* 57 (2001) 3644.
- [22] P. Schiebel, G.J. Kearley, M.R. Johnson, *J. Chem. Phys.* 108 (1998) 2375.
- [23] G. Voll, *Z. Phys. B* 90 (1993) 455.
- [24] J. Dornig, S. Flach, *Phys. Rev. B* 65 (2002) 214305.
- [25] W. Häusler, A. Hüller, *Z. Phys. B* 59 (1985) 177.
- [26] F. Fillaux, C.J. Carlile, G.J. Kearley, *Phys. Rev. B* 44 (1991) 12280.
- [27] A.C. Hewson, *J. Phys. C* 15 (1982) 3841.
- [28] M. Prager, J. Stanislawski, W. Häusler, *J. Chem. Phys.* 86 (1987) 2563.
- [29] N. LeCalvé, B. Pasquier, G. Braathen, L. Soulard, F. Fillaux, *J. Phys. C: Solid State Phys.* 19 (1986) 6695.
- [30] F. Fillaux, C.J. Carlile, G.J. Kearley, *Phys. Rev. B* 58 (1998) 11416.
- [31] E. Kaiser-Morris, PhD. thesis, Université d'Orsay, 1997.
- [32] J.R. Carruthers, D.J. Watkin, *Acta Cryst. A* 35 (1979) 698.
- [33] A. Larson, *Crystallographic computing*, F.R. Ahmed, Copenhagen: Munksgaard, 1970, p. 291.